J. Physiol. (1976), **260**, *pp.* 279–314
With 16 *text-figures*
Printed in Great Britain

SPIKE INITIATION BY TRANSMEMBRANE CURRENT: A WHITE-NOISE ANALYSIS

BY HUGH L. BRYANT AND JOSÉ P. SEGUNDO

From the Department of Anatomy and the Brain Research Institute, University of California, Los Angeles, California 90024, U.S.A.

(*Received 28 July 1975*)

SUMMARY

1. Those features of a transmembrane current correlated with spike initiation were examined in *Aplysia* neurones using a Gaussian white-noise stimulus. This stimulus has the advantages that it presents numerous wave forms in random order without prejudgement as to their efficacies, and that it allows straightforward statistical calculations.

2. Stimulation with a repeating segment of Gaussian white-noise current revealed remarkable invariance in the firing times of the tested neurones and indicated a high degree of reliability of their response.

3. Frequencies (< 5 Hz) involved in spike triggering propagated faithfully for up to several millimetres, justifying intrasomatic current injection to examine spike initiation at the trigger locus.

4. Examination of current wave forms preceding spikes indicated that a wide variety could be effective. Hence, a statistical analysis was performed, including computation of probability densities, averages, standard deviations and correlation coefficients of pairs of current values. Each statistic was displayed as a function of time before the spike.

5. The average current trajectory preceding a spike was multiphasic and depended on the presence and polarity of a d.c. bias. An early relatively small inward- or outward-going phase was followed by a large outward phase before the spike. The early phase tended to oppose the polarity of the d.c. bias.

6. The late outward phase of the average current trajectory reached a maximum 40–75 msec before triggering the action potential (AP) and returned to near zero values at the moment of triggering. The fact that the current peak occurs in advance of the AP may be partially explained by a phase delay between the transmembrane current and potential. The failure of the average current trajectory to return to control values immediately following the peak argues for a positive role of the declining phase in spike triggering.

7. Probability densities preceding spikes were Gaussian, indicating that the average was also the most probable value. Although the densities were broad, confirming that spikes were preceded by a wide variety of current wave forms, their standard deviations were reduced significantly with respect to controls, suggesting a preferred status of the average current trajectory in spike triggering.

8. The matrix of correlation coefficients between current pairs suggested that spikes tended to be preceded by wave forms that in part kept close to the average current trajectory and in part preserved its shape.

9. The average first and second derivatives of spike-evoking epochs revealed that current slope and acceleration, respectively, were most crucial in the last 200 msec before spike triggering, and that these dynamic stimulus components were more important for a cell maintained under a depolarizing, rather than a hyperpolarizing bias.

10. A simple model of the spike-triggering system, consisting of a linear filter (first-order Wiener kernel) followed by a threshold device with 'dead-time', was quite accurate in predicting experimentally observed spike timings.

11. It is concluded that a number of stimulus parameters (polarity and amplitude, variability, slope, acceleration, temporal correlation) are relevant in spike-triggering, and that, for a particular stimulus (e.g. a post-synaptic potential), the absence of one feature may be compensated for by the presence of another.

INTRODUCTION

One way information is transmitted within a network of synaptically connected neurones is through action and synaptic potentials. The basic element of such a structure is the single synaptic junction with its corresponding pre- and post-synaptic neurones. From a systems-analytic viewpoint (Fig. 1*A*), the synapse (2) can be schematized as transforming the presynaptic discharge or input (1) into the post-synaptic discharge or output (3) (Bryant, Ruiz-Marcos & Segundo, 1973; Brillinger, Bryant & Segundo, 1976; Segundo, 1970). It is clear, however, that within this 'black-box' formulation there are several important smaller subsystems (Fig. 1*B*, 1–5), knowledge of which would facilitate understanding the larger one. Of the possible subsystems, we have chosen to examine that which converts transmembrane current-to-spike discharge (Fig. 1*B*).

The mechanism of spike triggering was investigated utilizing Wiener's technique for system identification (Wiener, 1958; Lee & Schetzen, 1965). This method prescribes the use of a Gaussian white-noise (GWN) stimulus as a probe in order to obtain a set of characterizing 'kernels' (see Methods) that model the system and can be used to predict the response to any input.

The nerve cell can be considered as a 'decision-making unit' that unceasingly resolves the alternative of whether to fire an AP or remain silent and bases its decision on several issues, e.g. recent presynaptic arrivals (p.s.p.s), endogenous rhythms, and its own spike-triggering characteristics. The role of presynaptic arrivals was analysed in some detail for

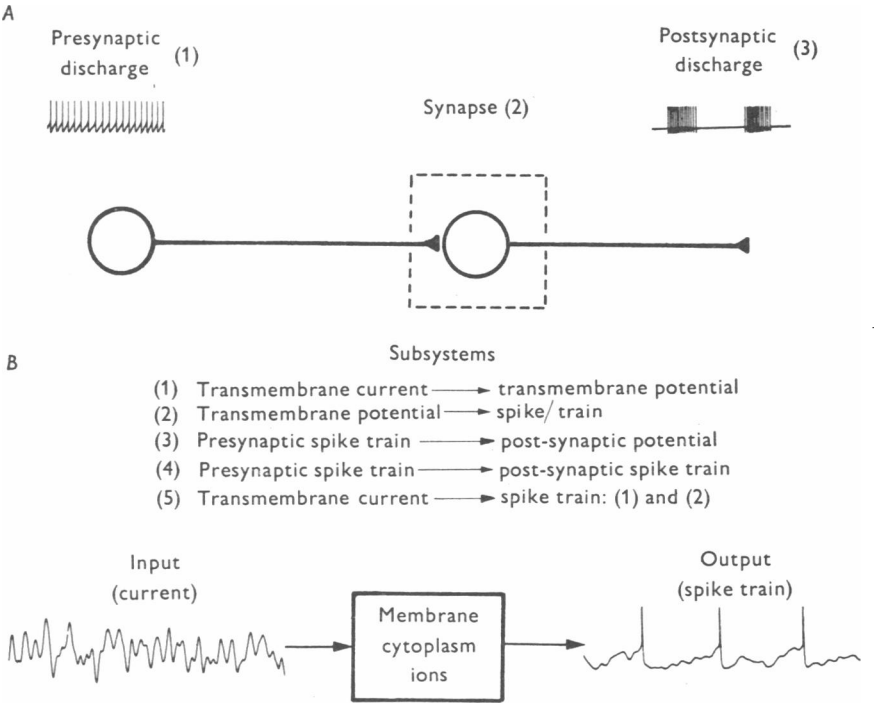

Fig. 1.*A*, Transformation of pre- to post-synaptic discharge. The synapse (2) may be viewed as a black-box which transforms a presynaptic discharge (1) as input into a post-synaptic discharge (3) as output. Within this formulation, several smaller black-boxes exist (*B*), e.g. the system which converts transmembrane current to spike discharge, a combination of subsystems (1) and (2).

a single cell receiving large e.p.s.p.s (Segundo, Perkel & Moore, 1966). It was also pointed out that two different questions can be raised in this situation: when the recent history is known, one asks for a prediction of whether the cell will fire or not; when the discharge behaviour is known, one asks for an inference concerning the recent history.

Both questions will be explored. This paper describes primarily the statistical features (average, variance, derivatives, correlation) of the spike-eliciting trajectories in the Gaussian white noise and their dependence on d.c. bias, i.e. the retrospective question of the features of the recent

currents given that an AP has just been initiated. Furthermore, it discusses efforts to model the current-to-spike triggering system using estimates of the first-order Wiener kernel. A preliminary report is available (Bryant & Segundo, 1975). A subsequent communication (H. L. Bryant, P. Z. Marmarelis, D. Brillinger & J. P. Segundo, in preparation) will describe the efficacy of different wave forms (from the Gaussian white-noise, rectangular and biphasic pulses, etc.) in eliciting APs.

METHODS

Experiments were performed on identified neurones (e.g. L1–L6, L10–L13, R2) of *Aplysia californica* abdominal ganglia, isolated with nerves and connectives in a Sylgard chamber, immersed in artificial sea water (ASW, pH 7·5–7·7) (Geduldig & Junge, 1968), and maintained at $17 \pm 1°$ C with a servo-controlled Peltier device. In order to facilitate cellular penetration in certain experiments with R2, the ganglion's sheath was softened by immersion in the enzyme Pronase (10 mg/ml.) for 10–15 min: procedure did not affect neuronal activity, although exposures of over 30 min did alter resting potentials, spontaneous firing and synaptic responses.

Cells were impaled with two separate electrodes (K citrate or KCl, 2–10 MΩ): a double-barrel electrode with one barrel for injecting a continually varying current and the other for passing a d.c. current; and a single-barrel electrode for recording. Intracellular recordings were obtained as described previously (Bryant *et al.* 1973). The continually varying current was modulated as Gaussian white noise. Theoretically, Gaussian white noise is characterized by a normal amplitude probability density, by a constant power spectrum over all frequencies, and by an autocorrelation zero everywhere except at the origin. The physical realization used had amplitudes that were normally distributed (but were truncated at ± 3 S.D. from the mean), was band-limited with constant power up to a certain frequency with a reasonably sharp cutoff of 25 db/octave. In initial experiments the Gaussian white noise was generated by a PDP-8/E computer system through the digital-to-analogue conversion of a sequence of normally distributed numbers stored on digital tape and read at rates which determined the noise bandpass. Subsequently, the Gaussian signal was produced by a Hewlett–Packard noise generator (Model 8057A) whose bandpass was determined by the frequency of an external clock. The Gaussian white-noise signal was then injected into the cell after passing through a voltage-to-current amplifier which, for a particular voltage, maintained a constant current independent of load resistance.

Preliminary experiments using sine wave stimuli indicated that frequencies over 5 Hz were ineffective (in the steady state) in eliciting APs in these neurones, with large cells typically having a narrower bandpass than small ones. Therefore, the high-frequency cutoff of the Gaussian white-noise current was usually set at 12·5 Hz (depending on the cell), more than twice the high frequency cutoff of the cell. The standard deviation of the Gaussian (σ_x) signal was pre-set so that when truncated at ± 3 S.D., the peak-to-peak current values ($\pm$ 10–100 nA, depending on the cell) produced transmembrane potential excursions of approximately ± 25 mV and/or over-all firing rates of 0·2–3/sec (see Fig. 2): these ranges exceeded somewhat the physiological ranges of subthreshold membrane potential oscillations and firing rates for these cells.

The Gaussian white noise was injected intrasomatically, though the locus of spike initiation (at least for cell R2) is approximately 1 mm from the soma (Tauc, 1962). It was therefore important to establish that influential components of the somatically

injected noise were not altered significantly in the process of electrotonic propagation to the spike-initiation point. The attenuation of each applied frequency with distance along the cell was studied in R2, a cell that allows impalement of the soma with stimulating and recording electrodes and of the axon with a third electrode for recording (Tauc, 1962). The between-electrode distance (from soma to axon) underestimates the actual cellular distances which could not be measured.

The time-invariance of the system was tested in several instances by observing the variability of the AP output of individual cells (L3, R2) to a particular sequence of Gaussian white noise of approximately 30 sec duration applied repeatedly for up to $1\frac{1}{2}$ hr. Additionally, the interval statistics (mean, S.D., autocorrelation) of the output spike train were compared during successive, non-overlapping segments (e.g. first 1/3, middle 1/3, final 1/3) to further verify the response stationarity and the time-invariance assumption.

Records on analogue tape (Hewlett–Packard 3960) of the Gaussian white-noise current input and transmembrane potential were obtained for subsequent computer processing and analysis.

White-noise analysis and computer processing

Wiener (1958) established that the output $Y(t)$ of a finite-memory, time-invariant non-linear system whose input $X(t)$ is a Gaussian white-noise process could be described by a series expansion of the form:

$$Y(t) = \sum_{n=0}^{\infty} G_n\{h_n, X(t)\}. \tag{1}$$

The G_ns are orthogonal functionals which depend upon the functions in parentheses; h_n is referred to as the nth-order Wiener kernel. The first three functionals are:

$$\left.\begin{aligned} G_0 &= h_0, \\ G_1 &= \int_0^{\infty} h_1(\tau)\,(t-\tau)\,d\tau, \\ G_2 &= \int_0^{\infty}\int_0^{\infty} h_2(\tau_1, \tau_2)\,(t-\tau_1)\,(t-\tau_2)\,d\tau_1 d\tau_2 - P\int_0^{\infty} h_2(\tau, \tau)\,d\tau. \end{aligned}\right\} \tag{2}$$

P is the power density spectrum of the input white noise. The constant G_0 reflects the over-all steady-state mean around which the system fluctuates. The convolution integral G_1 reflects the linear sum at time t of the effects of the inputs at all earlier instants $(t-\tau)$. G_2 describes quadratic behaviour and its leading term, a double integral, reflects how the output at time t is affected by the interaction of two inputs at different earlier instants $(t-\tau_1, t-\tau_2)$. Eqn. (1) and the Wiener kernels can be used to predict the system's response to any arbitrary input.

Lee & Schetzen (1965) demonstrated that, provided the system is probed with a Gaussian white-noise input, the kernels h_n could be obtained by relatively straightforward cross-correlational techniques. Thus,

$$h_0 = \overline{Y(t)}, \tag{3}$$

$$h_1(\tau) = \frac{1}{P}\overline{Y(t)\,(t-\tau)}, \tag{4}$$

$$h_2(\tau_1, \tau_2) = (2P^2)^{-1}\overline{\{Y(t)-h_0\}\,(t-\tau_1)\,(t-\tau_2)}, \tag{5}$$

where the bar indicates a time average of the quantity below.

In the present experiments we restricted our concern to the issues which result in spike initiation and, therefore, treated the output as a sequence of unit delta functions (see de Boer, 1967 for a similar technique) at the times t_i ($i = 1, \ldots, N$) of occurrence of the N spikes elicited by the Gaussian white-noise current (Fig. 2*A*):

$$Y(t) = \sum_{i=1}^{N} \delta(t-t_i), \tag{6}$$

where

$$\delta(t-t_i) = \begin{cases} 1, \text{ if } t = t_i \\ 0, \text{ otherwise.} \end{cases}$$

For an experiment of total duration T, the zero-, first- and second-order kernels become:

$$h_0 = \overline{Y(t)} = N/T, \tag{7}$$

$$h_1(\tau) = \left(\frac{h_0}{P}\right) \frac{1}{N} \sum_{i-1}^{N} X(t_i-\tau), \tag{8}$$

$$h_2(\tau_1, \tau_2) = (2P^2)^{-1} h_0 \left\{ \frac{1}{N} \sum_{i=1}^{N} X(t_i-\tau_1)X(t_i-\tau_2) - R(\tau_1-\tau_2) \right\}. \tag{9}$$

Thus, the zero-order kernel is the cell's over-all firing rate. The first kernel at τ is simply proportional to the average spike-eliciting current τ time units before the AP. The second kernel reflects certain average second-order properties of the current preceding a spike and is proportional to the covariance between current pairs. ($R(\tau)$ is the auto-correlation of the Gaussian white-noise input $X(t)$.) By defining the output as in (6), not only is computation of the kernels simplified, but their interpretation in biological terms is facilitated as each is a simple and physiologically meaningful transformation of the current leading to a spike (see Discussion).

One of the major purposes of obtaining the Wiener kernels *per se* is to generate a model which can be used in a predictive way to be compared with the biological system's behaviour. Our major purpose in this communication, however, has been to extract qualitative insights concerning spike generation. Accordingly, we have performed certain analyses which were likely to provide such insights irrespective of their relation to traditional Wiener analysis. Interestingly, two measures which we have found revealing (average spike-evoking current trajectory and correlation matrix of input values at two different times) resemble closely, but are not identical to, the first- and second-order Wiener kernels (eqns. (8) and (9)). The results of these experiments are most easily understood if one views them in the following simple terms. By stimulating the cell with a (non-repeating) Gaussian white-noise current stimulus, we have essentially provided the cell with many stimulus wave forms. Individual current wave forms will be referred to as 'trajectories', spike-eliciting if they precede a spike. Each epoch of noise which precedes an AP is distinguished from the noise in general and contains a certain, if small, amount of information about those processes involved in spike initiation. By subjecting these special spike-evoking noise epochs to a variety of (mainly) statistical analyses, we shall attempt to extract the relevant information.

Average spike-eliciting current trajectory (*ACT*)

The first and most obvious analysis to perform was the average of all the spike-evoking trajectories. Such an average is, except for the constant of proportionality h_0/P, identical to the first-order Wiener kernel (eqn. (8)). Our null hypothesis was

that the imposed current and the generated APs were independent events, i.e. their cross-correlation function was zero at all delays. The cross-correlation between the APs and the current at a particular delay τ was estimated by the sample mean

$$S_\tau = \frac{1}{N}\sum_{i=1}^{N} X(t_i - \tau) \tag{10}$$

of the currents $X(t_i-\tau)$ (see Fig. 2*B*) observed τ msec before each of the N APs occurring at times t_i. Under the null hypothesis of independence, each $X(t_i-\tau)$ has the distribution of the Gaussian white noise; i.e. is normal with mean 0 and variance σ_X^2 (see above). Moreover, it is reasonable to accept that the current values $X(t_i-\tau)$ for successive t_is in the sum are independent since the time lags for which the Gaussian white-noise values are correlated with each other (i.e. for which the Gaussian autocorrelation is not zero) are extremely short compared to the intervals (equal to those between spikes) from one t_i to the next. Hence, the central limit

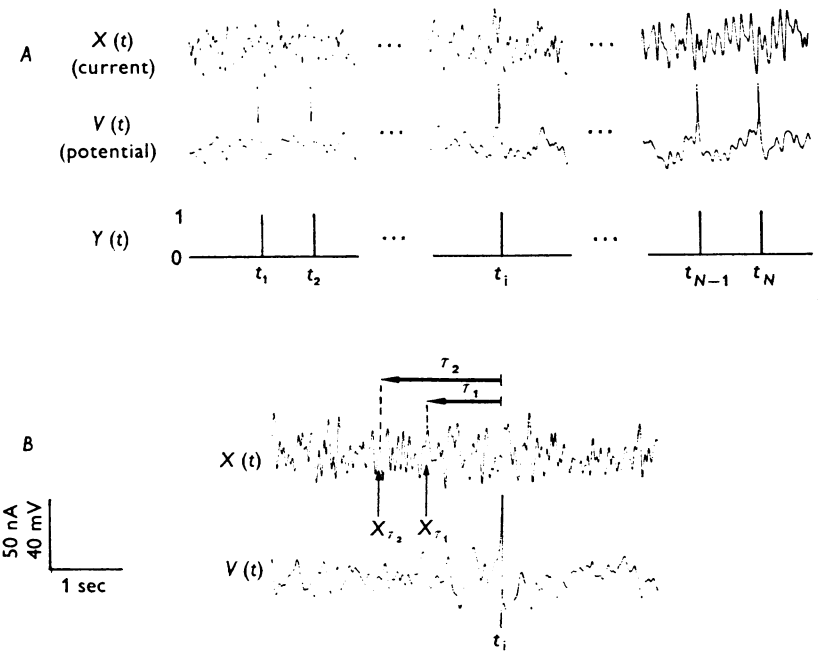

Fig. 2. Experimental and analytic paradigm. In *A*, a Gaussian white-noise-modulated transmembrane current, $X(t)$, injected intrasomatically through one electrode results in membrane potential oscillations and spike discharges, $V(t)$. The cell's output $Y(t)$ is regarded as a sequence of unit delta functions coincident with the times of occurrence t_i of the N spikes. In *B* the inputs (X_{τ_1}, X_{τ_2}) at two lags τ_1, τ_2 from the occurrence of a spike at t_i are shown. Values of the input at a single lag τ_1 are used to estimate the average current trajectory, distribution and standard deviation at that lag; values of the input at two lags τ_1, τ_2 are used to estimate correlation matrices.

theorem (Feller, 1966) stipulates that, as N increases, the distribution of the normalized sums

$$S_\tau^* = \frac{1}{\sigma_X \sqrt{N}} \sum_{i=1}^{N} X(t-\tau_i)$$

tends to the Gaussian with mean 0 and variance 1. Because the sample mean S_τ equals S_τ^* times $\sigma_X/\sqrt{N}$, its distribution tends to the Gaussian with mean 0 and variance σ_X^2/N. Hence, the confidence limits for the average current trajectory (S_τ) can be based upon this known distribution. We chose the approximately 96th percentile band provided by 2 S.E.s on each side of the mean, where 1 S.E. $= \sigma_X/\sqrt{N}$. One definition of the 'memory' of the current-to-spike generating system, then, is the distance from the spike to the point in negative time where the average current trajectory emerges from the confidence band (Fig. 6).

Variance and density function of the spike-eliciting trajectories

The ACT is an average wave form and therefore only a partial answer to the retrospective question of which trajectories precede an AP: it thus leaves other questions open. A very crucial one is that of the relative frequencies with which APs were triggered by each trajectory, i.e. of the likelihood of the different wave forms given that an AP has occurred, and several aspects of it were examined. Note that this question is not identical to the prospective one of the effectiveness of each particular wave form in eliciting an AP, i.e. of the likelihood of an AP given that a certain trajectory was generated. This must be stressed because confusion of one approach with the other is not uncommon and may be misleading.

The probability density of the current values at each of several particular τ delays staggered with respect to the AP can provide insights into the triggering process (Bryant & Segundo, 1975). The density was estimated by the histogram of the set $\{X(t_1-\tau), \ldots, X(t_N-\tau)\}$ of current values at each τ. Tests for normality were performed on the density function using the χ^2 test of goodness of fit (Dixon & Massey, 1969) and on the distribution function using the Kolmogorov–Smirnov test (Massey, 1951). The average current trajectory at each τ preceding a spike is the mean (S_τ) of the distribution of current values at that lag.

A second important parameter is the standard deviation, $\sigma(\tau)$, which reflects the dispersion of the individual current values around the average current trajectory at each τ. Under the null hypothesis of independence of Gaussian white-noise current input and AP generation, $\sigma(\tau)$ should not differ from the standard deviation σ_X of the over-all Gaussian white noise. The sampling distribution of standard deviations follows the χ^2/degrees of freedom (χ^2/df) distribution (Dixon & Massey, 1969, p. 102) with 98% confidence limits given by:

$$\alpha\sigma_X < \sigma(t_i-\tau) < \beta\sigma_X,$$

where

$$\alpha = (1-2/9N-2{\cdot}326\sqrt{2/9N})^{\frac{3}{2}},$$

$$\beta = (1-2/9N+2{\cdot}326\sqrt{2/9N})^{\frac{3}{2}}.$$

First and second derivatives of effective spike-evoking epochs

The role of the gradient of a stimulating current in processes associated with spike generation (e.g. accommodation) has long been recognized (Lucas, 1907). We computed the average first and second derivatives of the effective spike-evoking epochs as a function of τ to assess the roles of stimulus slope and acceleration at various moments prior to AP initiation. Because the average first and second derivatives of

the spike-evoking epochs are equal to the first and second derivatives of the average current trajectory, we estimated these derivative functions by first digitally smoothing (degree 1, 5-point smoothing) and then numerically differentiating (2nd degree Lagrange polynominal) the average current trajectory once to obtain the average stimulus current gradient and twice to obtain the average stimulus current acceleration as a function of time prior to spike generation (Hildebrand, 1956).

Correlations of the input at two lags

The second Wiener kernel (eqn. (8)) provides an indication of how interactions of the input at two lags (see Fig. 2*B*) influence spike generation. We felt, however, that an alternative measure of second-order interactions – namely, the familiar correlation coefficient – would provide important physiological insights, be readily interpretable, and be easier to establish confidence measures for than would the second-order Wiener kernel. A matrix of correlation coefficients $\rho(\tau_1, \tau_2)$ – or for brevity ρ_{12} – was computed between the current inputs $X(t_i-\tau_1)$ and $X(t_i-\tau_2)$ at two different lags τ_1, τ_2 before a spike. By definition, the correlation coefficient between two random variables is equal to their covariance divided by their standard deviations

$$\rho(\tau_1, \tau_2) = \frac{\frac{1}{N}\sum_{i=1}^{N} X(t_i-\tau_1)X(t_i-\tau_2) - S_{\tau_1}S_{\tau_2}}{\sigma(\tau_1)\sigma(\tau_2)}, \tag{11}$$

where the sample means S_τ are given by eqn. (10) and $\sigma(\tau)$ is as previously defined. This expression resembles, but is not identical to, that for the second-order kernel (eqn. (9)). We establish a confidence interval by testing the hypothesis that $\rho_{12} = 0$, i.e. that the inputs at lags τ_1 and τ_2 are independent. For large N, the 98 % confidence level is approximately $|\rho_{12}| \cong 1{\cdot}960/\sqrt{N}$, where N is the number of APs.

Model of current-to-spike-triggering system

The Wiener kernels (h_n) can be used in conjunction with eqn. (1) to predict the system's response to an arbitrary input. By defining the output as a sequence of unit delta functions coincident with the occurrence of the Gaussian-evoked APs (eqn. (6)), we have effectively cascaded the current-to-spike triggering system with a threshold device (Fig. 3). This procedure offers several conceptual and computational advantages as previously discussed; however, the introduction of such a 'hard' non-linearity implies the presence of very high-order Wiener kernels. In view of this, we have made preliminary efforts to model the spike triggering system with the first-order linear kernel, $h_1(\tau)$, followed by a threshold device with a 'dead-time'. A long sequence of Gaussian current was used as input both to a nerve cell (R2)

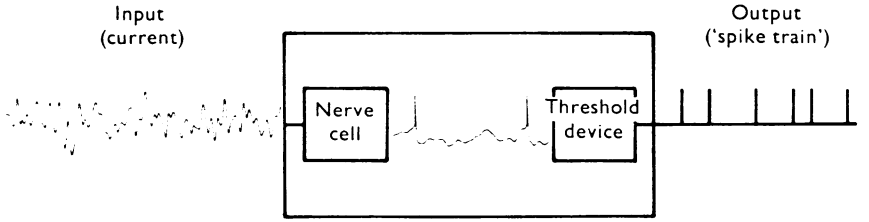

Fig. 3. Current-to-spike triggering system cascaded with a threshold device. The input to the system was Gaussian white-noise transmembrane current and the output a sequence of unit delta functions coincident with the occurrence of the elicited APs.

and to the linear kernel $h_1(\tau)$ for that cell estimated as previously described (eqn. (8)). The output $Y(t)$ from $h_1(\tau)$ was then fed into a threshold device with a dead-time: when $Y(t)$ exceeded a certain (arbitrary) value, then an impulse was generated. The 'dead-time' of the threshold device was also set arbitrarily to the minimum observed interspike interval (typically $\sim$ 200 msec) of cell R2 in response to the same Gaussian current input.

The AP timing of the cell and the impulse timing of the model were compared in terms of 'hits' and false positives and negatives. A 'hit' occurred when an AP from the cell and impulse from the model occurred within 30 msec of one another. A false positive is an impulse generated by the model when the cell was silent and a false negative occurred when an AP generated by the cell was not mimicked by the model.

RESULTS

System time-invariance and response to repeated Gaussian white-noise segments

For all data presented, the time-invariance of the system was established by ensuring that the spike-train interval statistics did not change with time (see Methods). Even in cells (e.g. L10, L7, L3) with strong endogenous or synaptic activity this requirement was almost always satisfied.

The remarkable time-invariance of these cells can be dramatically illustrated by injecting a repeating sequence of Gaussian white-noise current. Results with cell R2 are shown in Fig. 4 with the Gaussian current segment (repeated at 2–3 min intervals) in the bottom record and six response records above illustrating the near exactness of the response to such a repeated stimulus. The transmembrane potential fluctuations are virtually identical, and the AP timing is constant and precise with the exception of the fourth spike which occurred with one timing in records 1, 3 and 4 and slightly earlier in records 2, 5 and 6. This striking consistency was typical of other cells (e.g. L5) as well in which there is often little influence from other sources (p.s.p.s, pace-maker potentials). The presence of other sources of firing does not invalidate the Wiener analysis as long as they are uncorrelated with the Gaussian input (Marmarelis & Naka, 1973*a*). These data provide compelling support for the assumption of time-invariance (see Discussion).

Justification of intrasomatic current injection

To justify the analysis of spike initiation with intrasomatic current injection, we sought to determine the extent of spatial filtering between the soma and the probable region of spike triggering. Cell R2 was impaled with three electrodes, two in the soma for current injection and recording (upper trace in each pair in Fig. 5), and one in the axon for recording at varying distances (lower trace). The spike-trigger locus is somewhere between the somatic and axonal electrodes (Tauc, 1962).

For frequencies below 10 Hz, most filtering occurs in the conversion of somatic transmembrane current-to-potential. When a Gaussian white-noise current with a 12·5 Hz bandpass was injected into the soma (Fig. 5*A*, *C*), a slight filtering of the potential wave form from the somatic to the axonal electrode was seen at 5 (Fig. 5*A*), but not at 2 mm (Fig. 5*C*) away. When the noise bandpass was 50 Hz (Fig. 5*D*), a clear high-frequency filtering of the electrotonically propagating potential occurs. As indicated in Methods, however, spike initiation in these cells is not influenced by frequencies greater than 5 Hz. When a 1 sec rectangular pulse of inward current (Fig. 5*B*) was injected, there was almost no difference between the

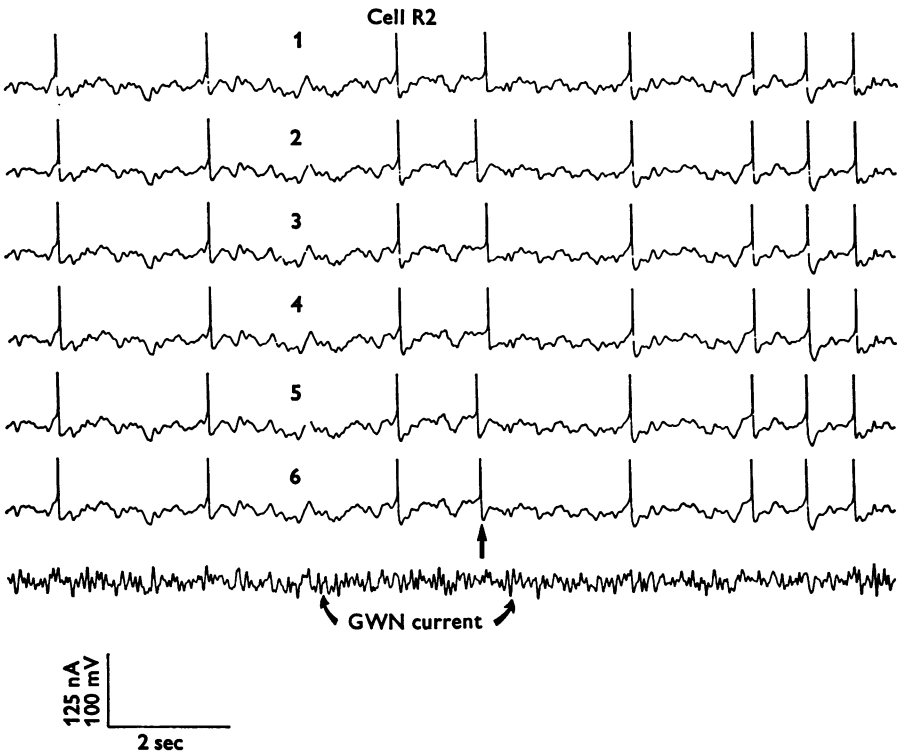

Fig. 4. Response of cell R2 to a repeating segment of Gaussian white-noise. The bottom trace is a 15 sec segment of Gaussian current (± 25 nA) which was repeatedly injected into R2 at 3–5 min intervals. Traces 1–6 show the response to six such identical stimulus sequences revealing a high degree of time invariance of the current-to-spike triggering system. The only variability in the response occurs at the arrow: the fourth spike in traces 1, 3 and 4, though occurring synchronously with one another, is slightly delayed with respect to the fourth spike in traces 2, 5 and 6. This result also suggests a high degree of reliability in the response of individual neurones to the presentation of an identical stimulus.

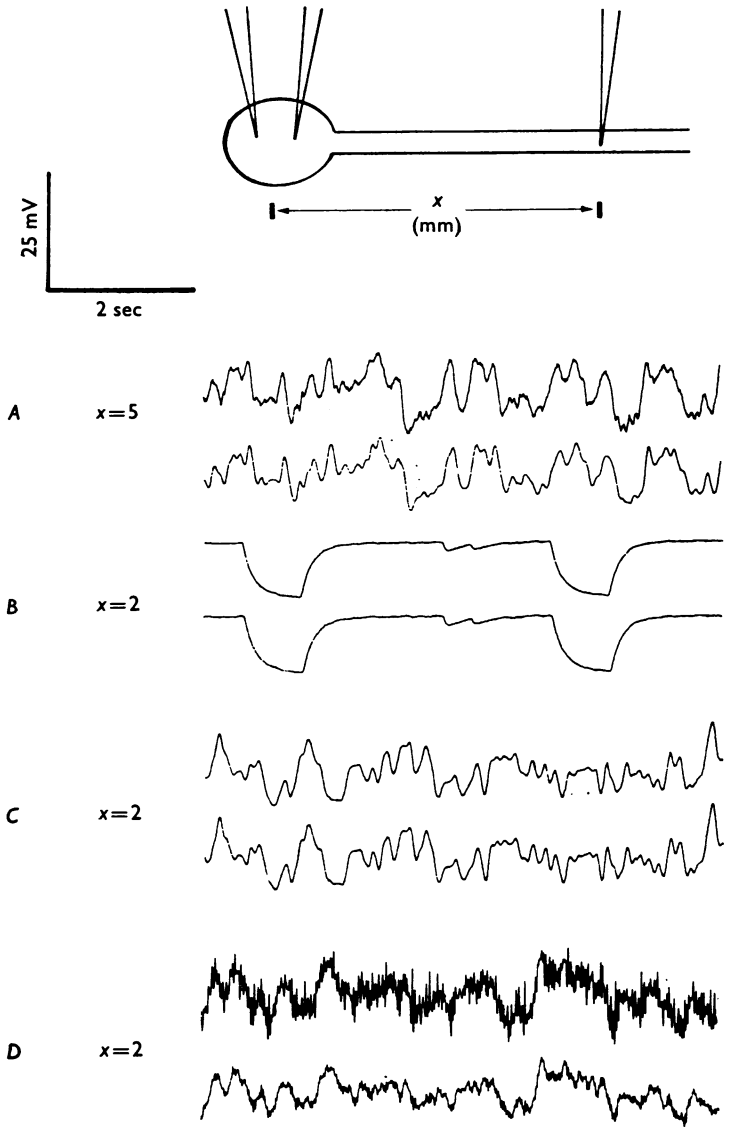

Fig. 5. Characteristic length as a function of frequency. Cell R2 was impaled with three electrodes, two in the soma for current injection and recording and a third recording electrode in the axon at varying distances from the soma. The upper trace of each pair is the somatic and the lower trace the axonal recording. At a distance of 5 mm (*A*) there is a slight low frequency filtering of the injected GWN current in the electrotonic propagation from soma to axonal electrode. At 2 mm (*B*), somatically-injected hyperpolarizing pulses and a 12·5 Hz GWN current (*C*) are only negligibly altered in propagation to the axonal electrode; at this distance, however, a GWN signal with a 50 Hz bandpass (*D*) is significantly filtered.

potential responses of soma and axon 2 mm away, and p.s.p.s recorded at both loci had nearly identical shapes and amplitudes (Fig. 5*B*). These results are compatible with a proposed space constant of nearly 1 cm for a d.c. signal (though see Tauc, 1962) and of several mm for frequencies up to 7 Hz. They justify intrasomatic current injection for these studies, providing the other cells where this control was not possible behave similarly. Graubard (1973) has also suggested a large space constant for these cells.

Average of the spike-evoking current trajectories

The average current wave form $S\tau$ which precedes a spike is closely related to the first-order Wiener kernel $h_1(\tau)$ as defined in eqn. (8) and corresponds to the impulse response function of the best linear model of the transmembrane current-to-spike triggering process. It is useful, in terms of its interpretation and of obtaining qualitative insights into spike initiation, to think of it accordingly. Fig. 6 shows the results of an experiment with cell L5 in which a Gaussian white-noise current (having a ± 25 nA range and a 12·5 Hz bandpass) was modulated about three different imposed d.c. biases: 10 nA hyperpolarizing in Fig. 6*A*, none in Fig. 6*B*, and 10 nA depolarizing in Fig. 6*C*. The time of occurrence of an AP at $\tau = 0$ is indicated by an arrow in the upper right, and negative time is measured to the left along the abscissae. The ordinate is in terms of nA of current, with values above 0 indicating outward or depolarizing current and those below indicating inward or hyperpolarizing current. The horizontal lines represent a 96% confidence band centered at the over-all average. By chance alone, a current value can fall outside this band with a probability of only 0·04.

A comparison of the average current trajectory in Fig. 6*A–C* indicates that the average of the effective stimulating epochs has features that do not change and features that do change as a function of the presence and polarity of an imposed d.c. bias. Hence, the set of spike-evoking epochs which the cell 'selects' from the ensemble is determined by the d.c. bias or mean. All trajectories in Fig. 6*A–C* have common aspects. First, they exhibit distinct early and late phases. The early phase starts between 650 and 300 msec and ends about 200 msec before spike initiation, exhibiting a small and slow current wave form which opposes the d.c. bias, i.e. is depolarizing in Fig. 6*A* and hyperpolarizing in Fig. 6*C*. The late phase starts about 200 msec before spike initiation and exhibits a relatively large and fast-rising peak of depolarizing current: this phase reaches a maximum, not at the moment of spike initiation, but roughly 60 msec earlier. The trajectories differ in other ways. First, the late depolarizing phase is slower in its rate of rise when the cell is hyperpolarized (Fig. 6*A*) than when it is

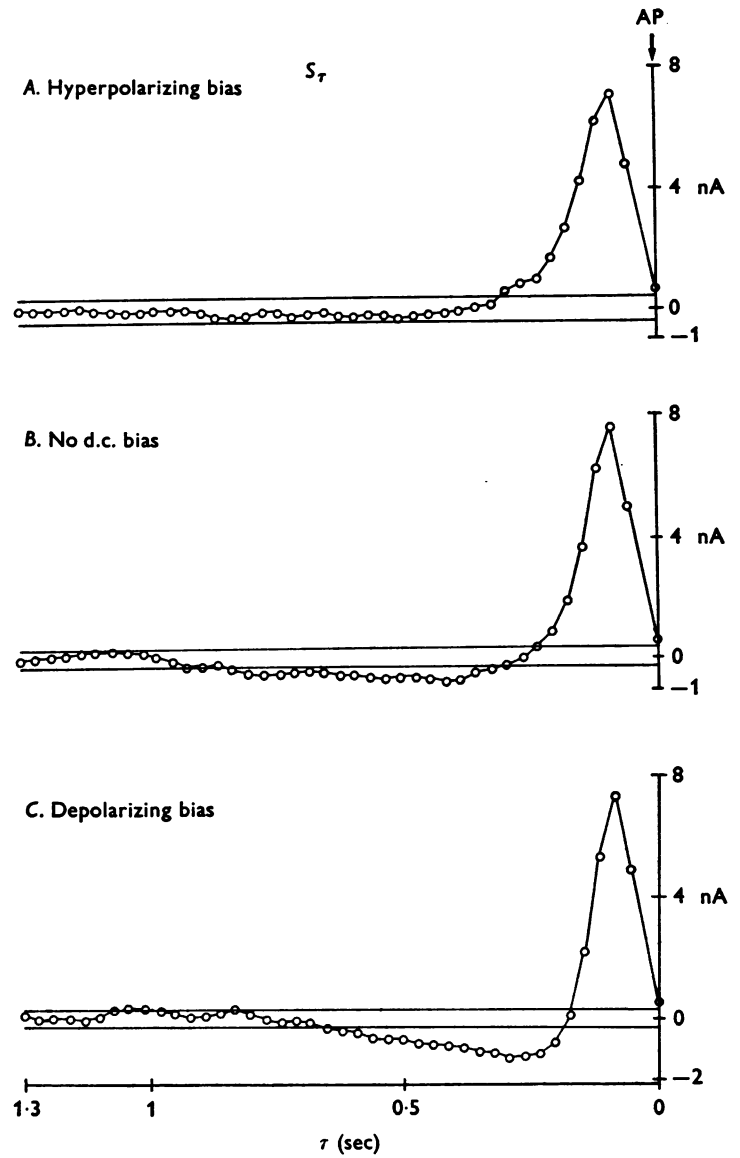

Fig. 6. Cell L5. Average current trajectory noise as a function of d.c. bias. A non-repeating Gaussian white-noise current (± 25, nA, 12·5 Hz bandpass) was injected into cell L5 held under a 10 nA d.c. hyperpolarizing bias (*A*), no bias (*B*) and a 10 nA d.c. depolarizing bias (*C*). The resultant average trajectories indicate that the cell selects a population of effective current trajectories which is determined by the presence and polarity of a d.c. bias.

depolarized (Fig. 6*C*) (see also below). Secondly, when the cell is hyperpolarized the average current trajectory emerges from the confidence band at about 300 msec before initiation, whereas when depolarized this occurs at 650 msec. The time between the emergence of the trajectory from the confidence band and spike initiation is one measure of the cell's 'memory', that is, the period of time during the stimulus history of a cell in which an input may influence spike initiation.

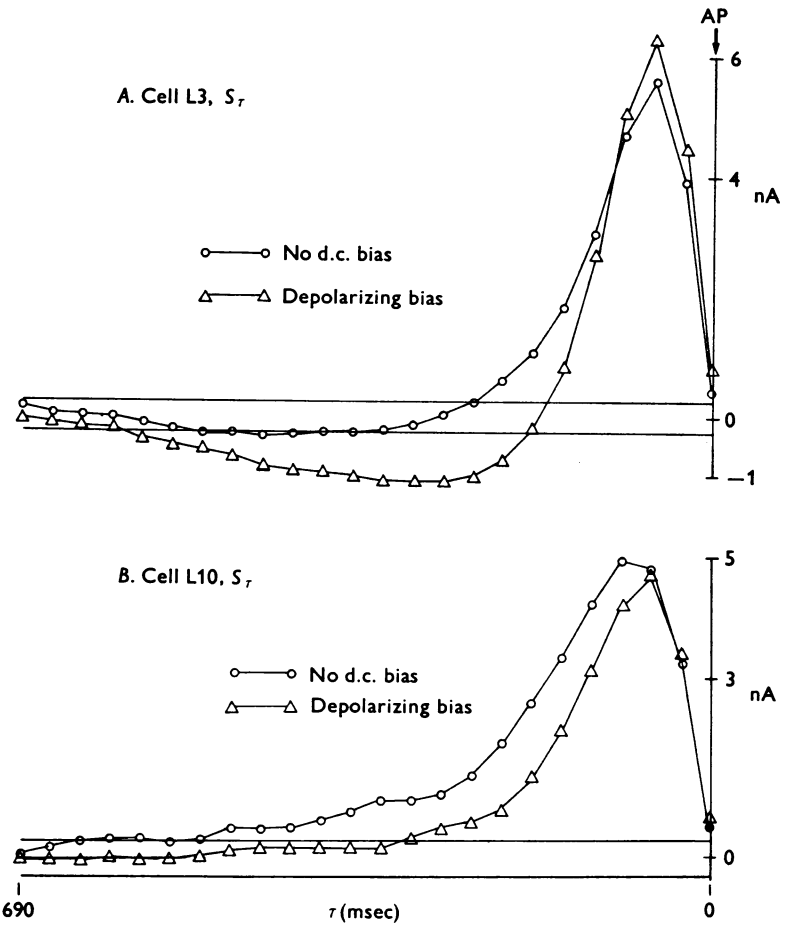

Fig. 7. The form of the average current trajectory depends on the net d.c. bias imposed on the cell. In *A*, a 10 nA depolarizing bias results in an average current trajectory with an early, slow hyperpolarizing phase. In *B*, a depolarizing bias (△——△) abolishes the early outward phase seen with no d.c. bias (○——○) but does not produce an early inward phase; this is presumably because the imposed depolarizing bias is added to other intrinsic or extrinsic sources of d.c. bias.

The form of the slow early phase depends on the d.c. bias. Increased hyperpolarizing biases result in more prolonged and larger early outward phases; increased depolarizing biases result in larger but usually briefer early inward phases (compare Fig. 6*A* and *B*). Fig. 7*A* shows average current trajectories obtained in cell L3 with no d.c. bias (circles) and with a 15 nA depolarizing bias (triangles); the depolarizing bias enhances the

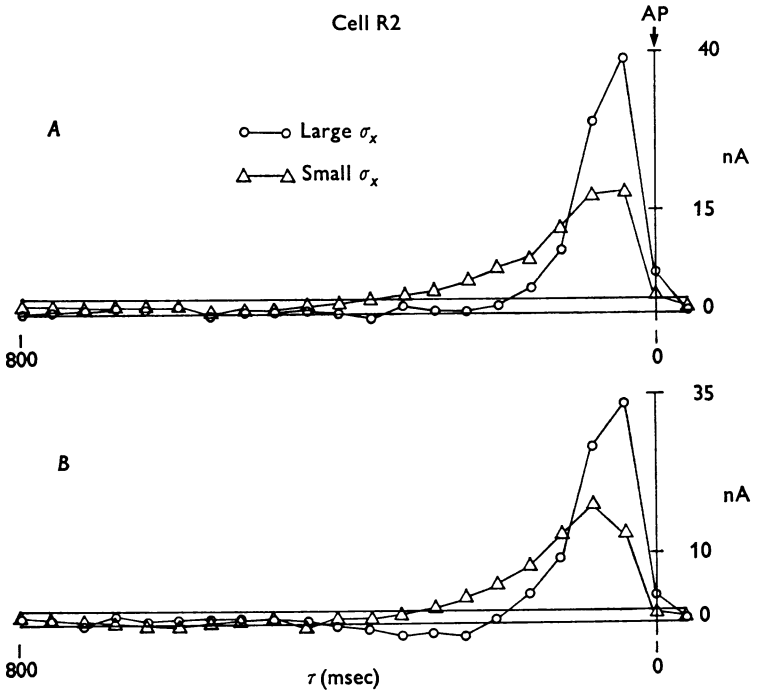

Fig. 8. Effect of σ_X on the form of the average current trajectory. Two experiments with cell R2 (*A* and *B*) were performed using Gaussian white-noise current with large and small standard deviations (σ_X = 30 and 15 nA, respectively). The form of the trajectory depends importantly on σ_X and is more prolonged with a slower-rising late outward phase when σ_X is small. An early inward phase (*B*) may also appear when σ_X is large.

early inward phase and produces a faster-rising late outward phase consistent with Fig. 6. Fig. 7*B* shows the results of a similar experiment with cell L10: notice that with a depolarizing bias (triangles) the slow early phase is outward, but is smaller and less prolonged than with no d.c. bias (circles). Thus, the exact form of the slow early phase depends on the net d.c. bias, that is, on the resultant of those biases imposed by the experimenter and on those imposed by other sources (e.g. synaptic, hormonal). The experimentally imposed bias may be small in relation to the others;

none-the-less, it is always true that a depolarizing bias tends to make the slow early phase inward (or less outward), and a hyperpolarizing bias makes it outward (or less inward).

The peak-to-peak amplitude excursions of the Gaussian current are determined by its standard deviation σ_x (see Methods). The influence of σ_x on the form of the average current trajectory was examined in several cells. The results of two such experiments with cell R2 are shown in Fig. 8*A*, *B* in which large (σ_x = 30 nA, open circles) and small (σ_x = 15 nA, open triangles) amplitude excursions were used. These experiments may also be viewed as indicating the form of effective spike-eliciting trajectories when large-amplitude excursions are less frequent. Under such conditions, i.e. when σ_x is small, the cell selects trajectories which, on the average, have a more prolonged, larger early phase and a slower-rising, smaller late outward phase. Additionally, Fig. 8*B* shows that when σ_x is large there can be a definite early inward phase, very much as though a depolarizing bias had been imposed. In spite of the very much larger maximum value in the average current trajectory when σ_x was large, the average charge delivered per AP (as reflected in the integral of the trajectory) was only 14 % greater than when σ_x was small (e.g. 1·80 *vs.* 1·55 nA-sec in Fig. 8*A*). These results argue for a role of the integral of the stimulus current in spike triggering.

Several aspects of the results of Figs. 6, 7 and 8 require further comment. The average current trajectories invariably reach a maximum between 40 and 75 msec before the moment of spike initiation and decrease rapidly to *near* zero at the time of triggering. Were the AP actually triggered at the current peak such that the value of the current were no longer relevant, then the trajectory would return immediately to the confidence band following the peak. This is so because the interval between adjacent points in the trajectory was chosen to be just greater than the period of autocorrelation of the Gaussian white noise. Therefore, it can be said with confidence that the cell tended to 'select' those current trajectories which reached a maximum roughly 60 msec before triggering and which declined to *near* zero values at the moment of triggering. A partial explanation for the early peak is that, for cells L3 and R2, the phase relationship between current and voltage is nearly constant and approximately 72° in the frequency range 1–20 Hz. In the range 2–5 Hz, which covers the frequency range of the late outward current phase, the delay between transmembrane current and potential is 100–40 msec. It is, therefore, conceivable that although the AP is not triggered at the current peak, it may be triggered at or near the potential peak. Finally, we have computed the average current trajectory for a current threshold model of spike triggering (with refractoriness) in which an AP is produced whenever the Gaussian current exceeds a particular value. For such a model the average current trajectory is very brief (< 40 msec), rises nearly instantaneously from the confidence band near the moment of triggering and falls again to zero immediately at $\tau = 0$. It is clear that the cells we have examined cannot be regarded as current threshold devices.

Current distribution and standard deviation

Fig. 9 shows, for cell L5 (Fig. 9*A*), histograms of current values at selected lags (τ = 100 and 470 msec) from the spike. The corresponding average current trajectory is shown at the upper left of Fig. 9*A* with small arrows indicating the times at which the histograms were computed. The

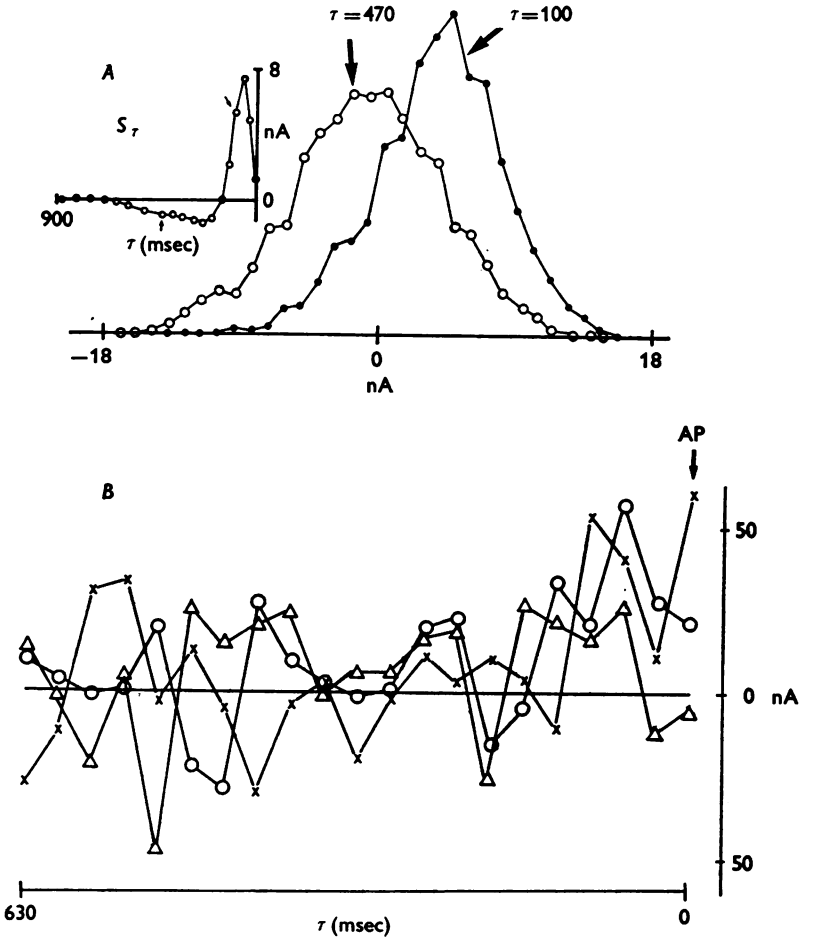

Fig. 9. *A*, distribution of current values at various lags before a spike. The average current trajectory for this data is shown in the upper left of *A* with small arrows indicating the lags (τ = 100 and 470 msec) corresponding to the distributions shown. The means and standard deviations of these conditional distributions clearly depend on τ. These distributions also indicate that the nerve cell is responsive to a variety of current trajectories; in *B* are shown three (digitized) individual current trajectories from an experiment with cell R2 which further illustrates this point.

histograms of current values conditioned on a spike remain compatible with the Gaussian distribution. Indeed, Kolmogorov–Smirnov tests indicated that 578 of the 592 distributions tested did not deviate significantly (at the 0·05 level) from normality. Of the fourteen deviant distributions, eight occurred within 100 msec of spike initiation. Deviant distributions still appeared symmetric and unimodal but seemed 'flatter' than expected, i.e. had fewer values near the mean and more at the tails. Although the conditional densities remain normal, their means and standard deviations clearly depend on τ.

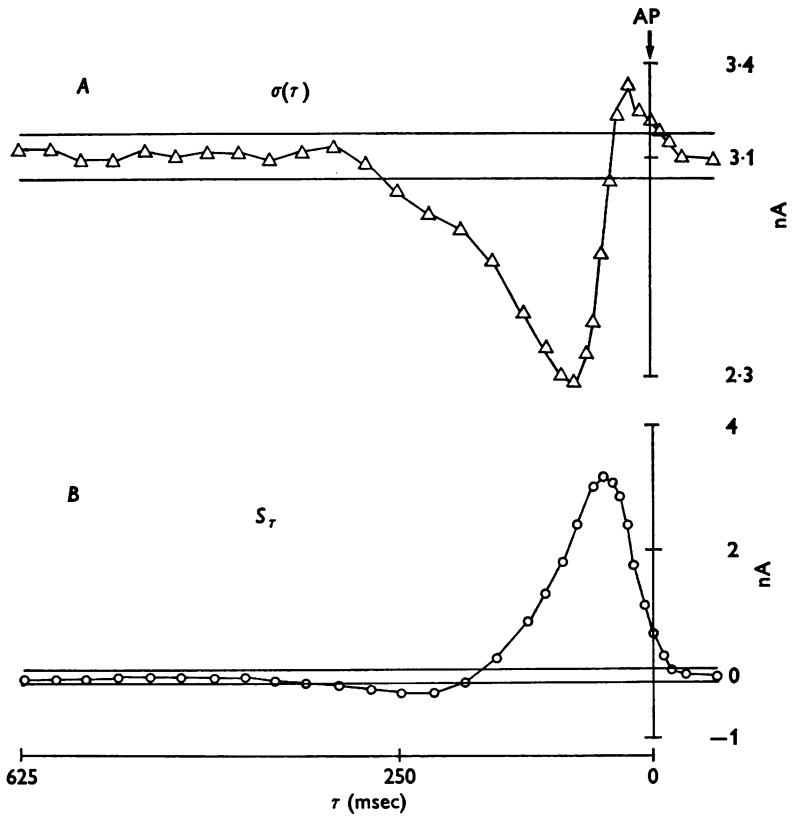

Fig. 10. Cell L10. Standard deviation of Gaussian white-noise current values as a function of τ. For cell L10 maintained under a 10 nA depolarizing bias, the average current trajectory (B; S_τ) exhibits an early hyperpolarizing phase. The standard deviation $\sigma(\tau)$ of current values at each τ preceding a spike (A) reflects the dispersion around the average current trajectory and decreases significantly from the overall standard deviation beginning at approximately τ = 300 msec, reaches a minimum at τ = 80 msec, and then exceeds control values at τ = 30 msec before returning to the 96 % confidence band. Ordinate values for the trajectory and for $\sigma(\tau)$ are in units of nA of current.

The histograms indicate that the AP is not preceded by a small set of very similar trajectories, and this point is further illustrated by the dissimilarities between the three individual (digitized) spike-evoking epochs (Fig. 9*B*) from an experiment with cell R2. These results emphasize that the nerve cell can respond to a wide variety of individual current trajectories.

Although the histograms conditioned on a spike are Gaussian in form, they are usually narrower than the controls implying reduced variability. Fig. 10 shows the standard deviation (Fig. 10*A*) and average current trajectory (Fig. 10*B*) as a function of τ for spike-eliciting currents in L10. The confidence band for $\sigma(\tau)$ is indicated as horizontal lines at the top of the Figure centered about the over-all standard deviation ($\sigma_x = 3{\cdot}1$ nA). The ordinate for both S_τ and $\sigma(\tau)$ is in nAs. At approximately the same time ($\tau = 350$ msec) that the trajectory (Fig. 9*B*) emerges from its confidence band, $\sigma(\tau)$ begins decreasing in relation to σ_x. This tendency continues and $\sigma(\tau)$ reached a minimum at approximately 65 msec before a spike. This minimum of $\sigma(\tau)$ does not correspond to the peak of the average current trajectory but, rather, occurs during the fast-rising late phase of outward current; this consistent result was true of over 90 % of our observations. At about 60 msec before the spike $\sigma(\tau)$ begins to increase rapidly, and just before initiation significantly exceeds σ_x. This greater-than-expected $\sigma(\tau)$ near the moment of spike initiation was also consistent and occurred about 70 % of the time. A reduction in $\sigma(\tau)$ with respect to σ_x indicates that the AP is preceded by noise epochs which tend to conform to the average current trajectory profile.

The use of a time-locked averaging procedure, such as that employed in this investigation, offers the advantage that the standard error for the estimated functions decreases with $\sqrt{N}$ so that an almost arbitrary level of accuracy can be obtained. For instance, in the data of Fig. 10, in which $N \cong 4300$ spikes were evoked by a Gaussian white-noise current with peak-to-peak excursions of ± 10 nA, the S.E. for the trajectory was 48 pA. Thus, although the early inward current phase of the trajectory never exceeds 300 pA, it was detected with a high degree of reliability ($P > 0{\cdot}001$). This implies that some membrane process is initiated by prehyperpolarization which contributes to spike initiation, and that this process is sensitive to currents of less than 300 pA: only an averaging technique could have revealed this with such sensitivity. These methods, therefore, offer the possibility of studying processes underlying spike triggering which were previously undetectable, even in cells which are spontaneously active and/or have a steady barrage of synaptic input.

The relationship between the average current trajectory and $\sigma(\tau)$ can be better appreciated if they are plotted with respect to one another (on abscissa and ordinate, respectively) in a Lissajou-like Figure with time as an implicit parameter whose direction is indicated by arrows (Fig. 11). The confidence bands for the trajectory and $\sigma(\tau)$ are indicated as pairs of

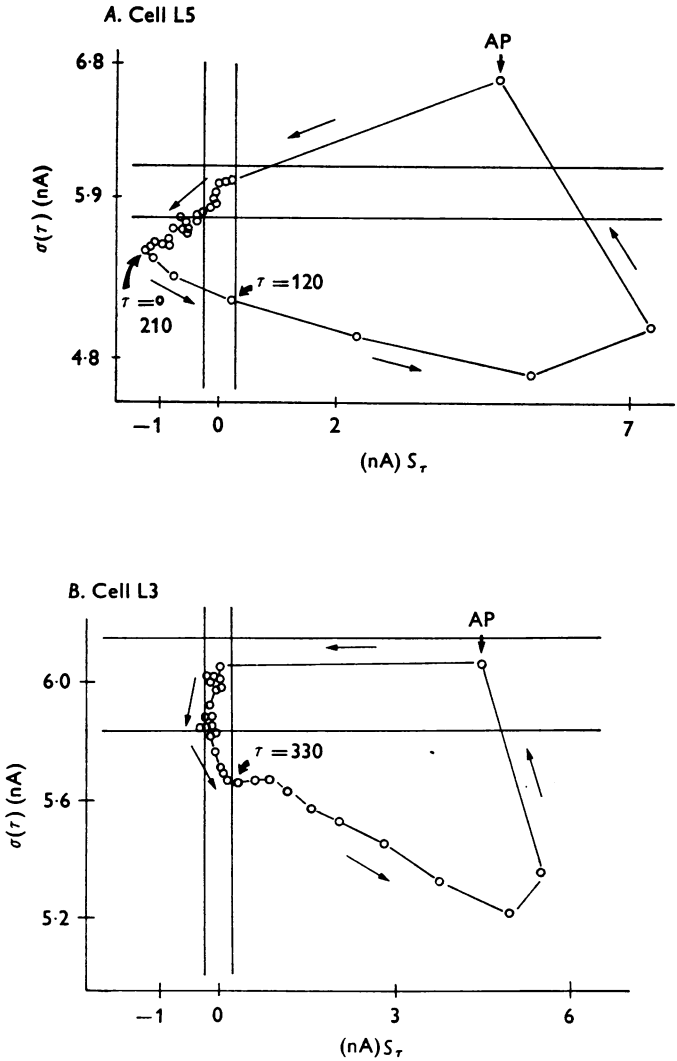

Fig. 11. Standard deviation as a function of average trajectory. Certain aspects of relationship between $\sigma(\tau)$ (ordinate) and the average current trajectory (abscissa) are better illustrated when they are plotted with respect to one another. Confidence bands for each are given by the vertical and horizontal lines, respectively. Time proceeds in a counterclockwise direction (see arrows) with closely spaced values indicating a relative stability or constancy in the relationship of $\sigma(\tau)$ to the trajectory and widely spaced values a rapidly changing relationship. In *A*, cell L5 was subjected to a depolarizing bias and in *B*, L3 was hyperpolarized (see text for discussion of details of Figure).

vertical and horizontal lines, respectively. When cell L5 is depolarized (Fig. 11*A*), both the average current trajectory and $\sigma(\tau)$ begin to emerge from their confidence bands simultaneously. In the early slow phase and from 700 to 210 msec before a spike, the small reduction in $\sigma(\tau)$ and the hyperpolarizing drift of the average current trajectory are seen as a scatter of very closely spaced points in the lower left quadrant. At $\tau = 210$ msec (see arrow) the two parameters begin to change rapidly with $\sigma(\tau)$ decreasing sharply as the trajectory enters the fast, late outward phase. This period is seen as the procession of distantly spaced points that move away from the lower left quadrant to the lower right ($\tau = 120$ msec) and finally, upper right quadrants. After spike initiation, points return to the intersection of the confidence bands.

Fig. 11*B* is a similar plot of average current trajectory *vs.* $\sigma(\tau)$ for cell L3 under a hyperpolarizing bias. During the period of 580–330 msec before a spike, $\sigma(\tau)$ was decreasing significantly but the trajectory had not yet emerged from its confidence band; this is indicated by a collection of points within the vertical but outside the horizontal confidence band. Note that in this particular case, $\sigma(\tau)$ did not exceed σ_x for $\tau < 60$ msec.

First and second derivatives (slope and acceleration) of effective epochs

The rate of rise of a stimulating current is relevant in spike initiation. In previous studies, analysis of its role was accomplished using current ramps which, since they have a constant slope, provide no information concerning the rate requirements at different times prior to spike-initiation. Fig. 12*B* shows the average slope of spike-evoking epochs as a function of τ for cell L5. The most striking feature of Fig. 12*B* is the difference of slopes in the last 100 msec before triggering when a cell under a depolarizing bias (circles) requires much larger slopes, i.e. faster-rising trajectories, than one under a hyperpolarizing bias (triangles) (80 and 50 nA/sec, respectively, at $\tau = 125$ msec). This period corresponds roughly to the late outward phase of the average current trajectories shown in Fig. 12*A*. Slightly earlier ($200 < \tau < 250$ msec), however, the slopes are greater in the hyperpolarized condition, indicating a need for a more prolonged (though slower-rising) flow of outward current just preceding a spike. Still earlier ($\tau >$ 200 msec), the slopes are very different. As indicated above, under a depolarizing bias epochs with a small (3–5 nA/sec on the average), negative (inward current) slope are preferred (Fig. 12*B*); whereas, under a hyperpolarizing bias the early outward phase was larger (5–9 nA/sec) but not as prolonged ($\tau =$ 360–200 msec). Fig. 12*B* also clearly shows that effective epochs reached a maximum slope a full 125 msec before spike initiation and had decreasing, even negative, slopes thereafter.

It is necessary to exercise caution when interpreting second derivatives

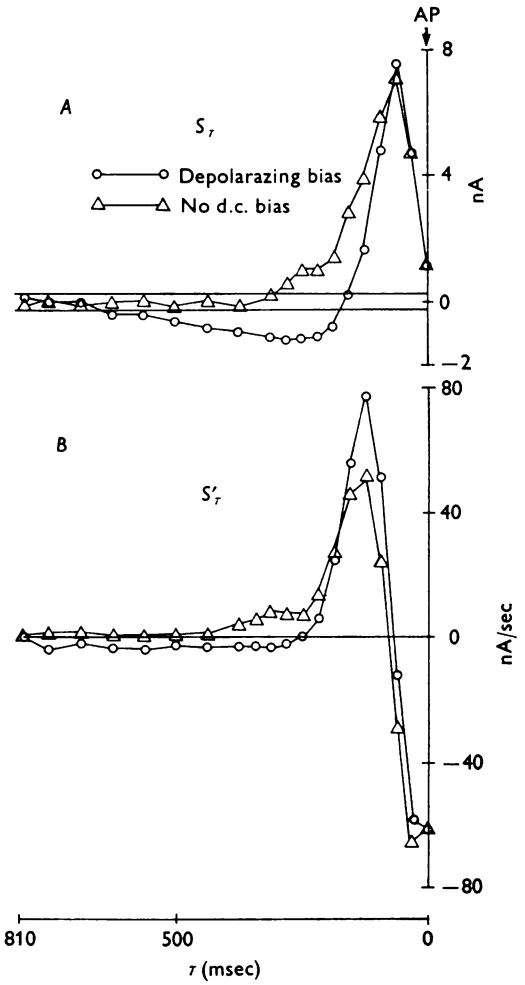

Fig. 12. Average slope of spike-evoking trajectories. In *A*, the average current trajectories for cell L5 maintained under a depolarizing (○——○) and hyperpolarizing (△——△) bias, and in *B*, the corresponding average slopes as a function of τ. With a depolarizing bias much faster-rising outward current trajectories are required in the critical period of 100–175 msec before spike initiation. Earlier in time (τ > 200 msec) small, nearly constant slopes, i.e. linear ramps of ~ 5 nA/sec, are required which are opposite in polarity to the imposed bias. The slopes actually begin to decrease very sharply at τ = 120 msec and become negative in the last 65 msec before spike initiation.

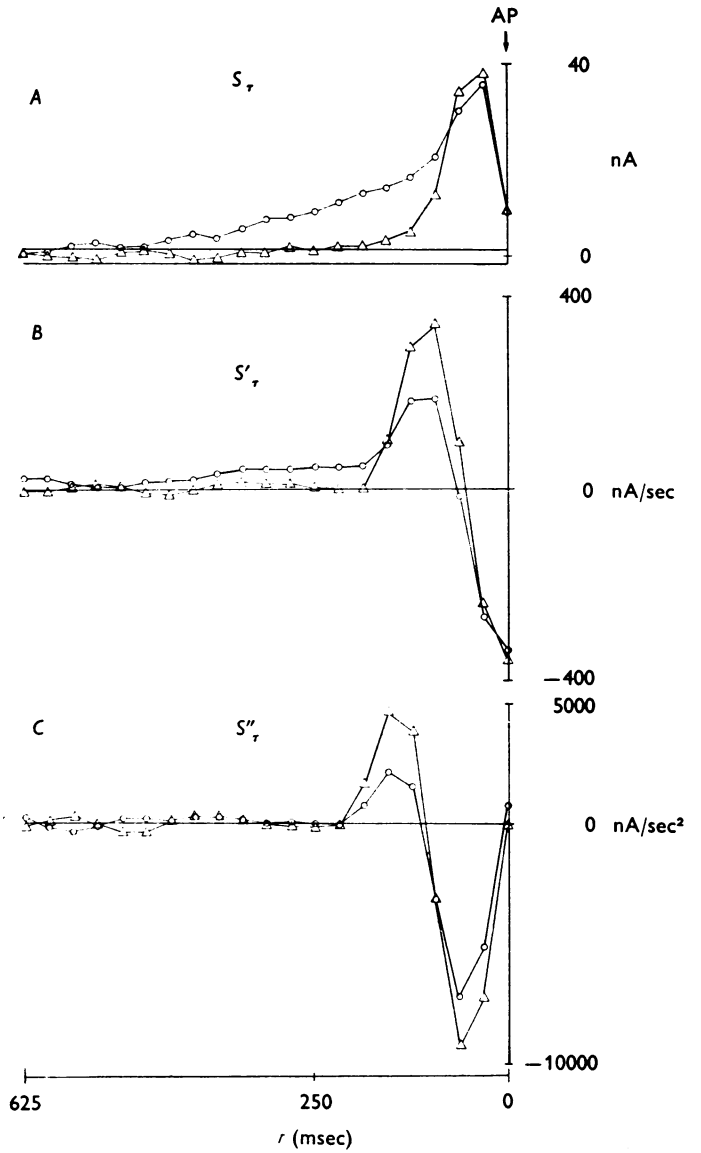

Fig. 13. Cell R2. Average slope and acceleration of spike-evoking trajectories. The average current trajectory (*A*), average slope (*B*), and average acceleration (*C*) for cell R2 under a depolarizing (△——△) and hyperpolarizing (○——○) bias are shown. The depolarizing bias eliminates the early, slow outward current phase of the average current trajectory produced by the hyperpolarizing bias. The requirement for faster-rising current slopes during the last 150 msec before triggering the action potential when the cell is depolarized is particularly evident (*B*). A depolarizing bias also imposes a requirement for faster-accelerating trajectories during the final moments before triggering (*C*), but effective trajectories had no acceleratory component earlier and were clearly decelerating during the final 75 msec.

obtained numerically, and we shall here concentrate only on the most prominent aspects of such computations. Fig. 13 illustrates an experiment with R2 under a 10 nA depolarizing (circles) and hyperpolarizing (triangles) bias showing the average current trajectories (Fig. 13*A*) and the corresponding average first (Fig. 13*B*) and second (Fig. 13*C*) derivatives, i.e. slopes and accelerations. Of particular interest is the prolonged early outward phase when the cell is hyperpolarized. The average current trajectories and average slopes (Fig. 13*A*, *B*) support the results indicated above (Figs. 6, 7, 12). The plots of second derivatives (Fig. 13*C*) indicate that under both bias conditions, acceleratory input current components are relevant only during the last 210 msec before spike initiation. It is also clear that under a hyperpolarizing bias large dynamic components are not as crucial (2200 *vs.* 470 nA/sec^2 at τ = 160 msec). Moreover, following the peak of acceleration at τ = 160 msec, and particularly in the last 100 msec, effective epochs were decelerating very rapidly.

Second-order associations in effective epochs

The matrix of correlation coefficients (Figs. 14 and 15) revealed second-order properties of the effective spike-evoking epochs. Each entry ρ_{12} in the matrix indicates how deviations of the input current from the average current trajectory at a particular lag τ_1 are associated with deviations at another lag τ_2 for those current trajectories which were effective. The matrix is symmetric, i.e. $\rho_{12} = \rho_{12}$, and only half of it need be shown. Diagonal elements (ρ_{11}) are equal to unity since the current for a particular lag is perfectly correlated with itself. Only those matrix entries that were significant at the 0·02 level or greater are shown: blanks are inserted for insignificant entries. We further abstracted the matrix by inserting a '+' and '−' in place of significant entries which were positive or negative, respectively (see Figs. 14 and 15). Because the correlation matrix reflects the association of deviations of the input current from the trajectory at two different lags, the trajectory has been placed along the τ_1 and τ_2 axes to facilitate interpretation.

Fig. 14 shows a correlation matrix for cell L10 under a depolarizing bias. The upper left corner corresponds to τ_1 and τ_2 large ($\sim$1 sec), the lower left to τ_1 large and τ_2 small, and the lower right to τ_1 and τ_2 small. There are three distinct matrix regions with significant correlations: (1) the lower right region indicates that input current values at small lags (i.e. during the late outward phase of the average current trajectory) are negatively correlated with one another; (2) the lower left region indicates that those at small lags are positively correlated with those at larger lags (i.e. during the early inward phase); and (3) the central region indicates that those at large lags are either positively or negatively correlated with one another.

The positive correlatien coefficients between the inputs during the late outward and early inward phases of the trajectory were homogeneous and exceeded the critical value for significance at the 0·02 level by a factor of 2 or 3 at most. These positive correlations imply, for instance, that an individual spike-evoking trajectory more (less) hyperpolarizing than the

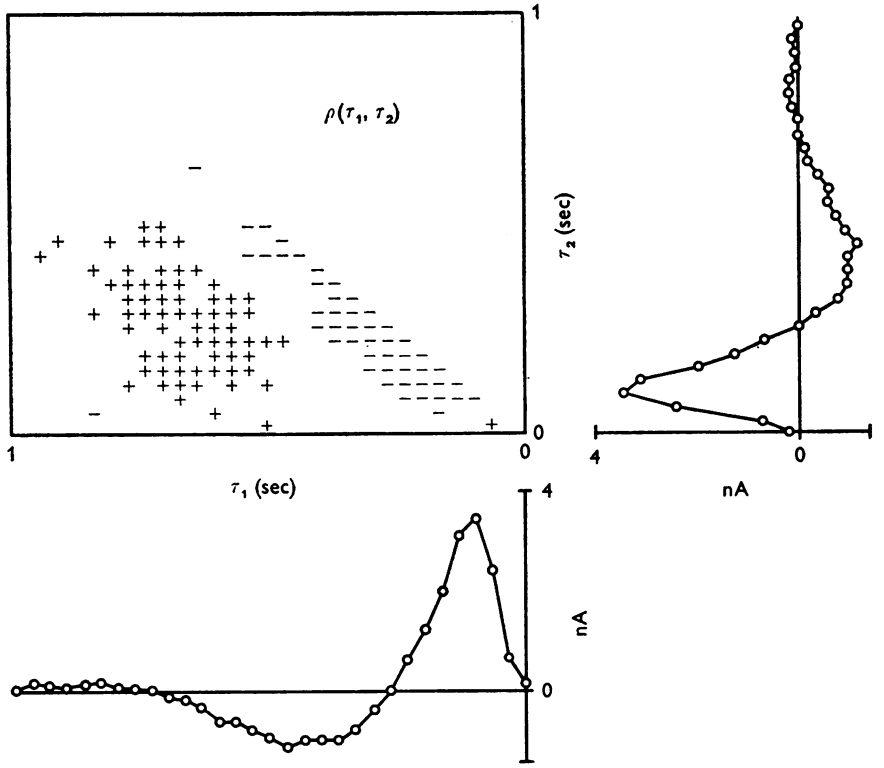

Fig. 14. Matrix of correlation coefficients for cell L10 under a d.c. depolarizing bias. The correlation coefficient matrix $\rho(\tau_1, \tau_2)$ between current pairs at various lags before an action potential is shown with the corresponding average current trajectories on the τ_1 and τ_2 axes. Only those coefficients which were significant at the 0·02 level are indicated (see Methods).

average current trajectory during the early inward phase, would most likely be less (more) depolarizing than the trajectory during the late outward phase. Such positive correlations between the early inward and late outward phases also imply a preservation, within individual trajectories, of a profile similar to that of the average current trajectory.

The negative correlation coefficients between input current values during the late outward phase exhibit a greater range than the positive

correlations: in general, they tend to be larger and increase dramatically as the moment for spike initiation approaches. It is not unusual for these negative coefficients to be 5 to 10 times greater than the critical value for significance at the 0·02 level. Such negative correlations during the late outward phase imply that a greater (less)-than-average depolarization at

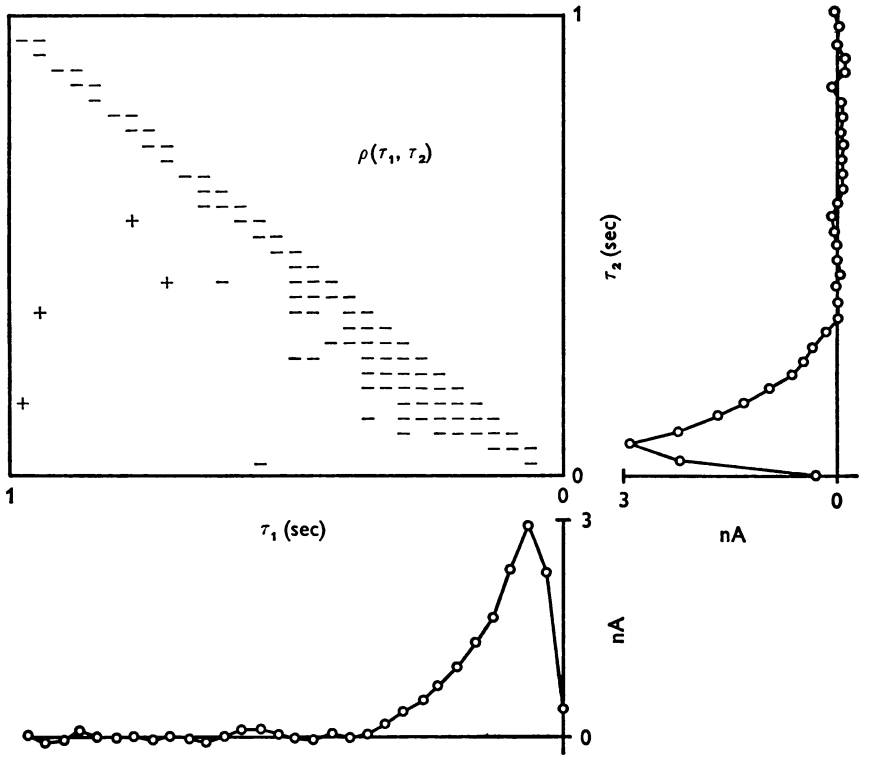

Fig. 15. Matrix of correlation coefficients for cell L1 with no d.c. bias. This matrix has essentially only negative entries corresponding to current pairs at short delays (τ = 250 msec) and to adjacent and near-adjacent current pairs at all delays (i.e. off-diagonal elements). Note that the 'memory' for second-order interactions exceeds that for first-order effects.

one moment would tend to be associated with a less (greater)-than-average depolarization at other moments. In other words, individual trajectories tend on the average to remain close to the average current trajectory. Because pairwise negative correlations exist during the late outward phase, and because their magnitude increase sharply as spike initiation approaches, it is clear that the slope of individual trajectories is very critical during this period and becomes increasingly so as τ approaches 0. Thus, the positive correlations between the early inward and late outward

phases and the negative correlations within the late outward phase both tend to emphasize the preferred nature of the average current trajectory in spike initiation, as both imply a tendency of the cell to respond to epochs which conform to it.

A mixture of positive and negative correlations exists between input values during the early hyperpolarizing phase of the trajectory. During the first part of the early phase when its slope is negative, input values are positively correlated; and during the second part of the early phase when its slope is positive (i.e. just before the late outward phase), input values are negatively correlated. The interpretation of these positive and negative correlations is as discussed above.

For a hyperpolarized cell with a slow, depolarizing early phase (Figs. 6, 7 and 13), significant entries in the correlation matrix are predominantly negative (Fig. 15): input values in the late outward phase are correlated negatively with others in both the late and earlier phases. Additionally, adjacent and near-adjacent (off-diagonal entries) input current values are negatively correlated for all lags out to $\tau = 1$ sec. The average current trajectory, on the other hand, begins to emerge from its confidence band at approximately $\tau = 350$ msec. Thus, the 'memory' for second-order interactions is greater than that for first-order effects. As with the data of Fig. 14, the negative coefficients within the late outward phase are large and increase sharply as τ approaches 0: they imply that deviations of the input above or below the average current trajectory at one moment are associated with opposite deviations at other moments. These correlation matrices demonstrate that there are systematic pairwise correlations between current values at different lags for input sequences which elicited spikes, and that the nature of these correlations depends on the cell's d.c. bias.

A model of the spike-triggering system

We have modelled the spike-triggering system using the first-order Wiener kernel $h_1(\tau)$ followed by a threshold with a dead-time (Fig. 16) or absolute refractory period. The top of Fig. 16 shows schematically the testing procedure in which the same current input is applied to the model and to the nerve cell. The model and nerve cell outputs were evaluated in terms of AP timing. Three continuous records of the AP timing of the cell ($\times$'s) and the model (open circles) are shown at the bottom of Fig. 16 and indicate an agreement that is quite excellent for such a simple model. In over 40 min of data, involving more than 650 APs in each record, the model accurately predicted the cell's AP timing 68 % of the time while producing 24 % false positives (spurious impulses generated by the model which had no relation to the cell's behaviour).

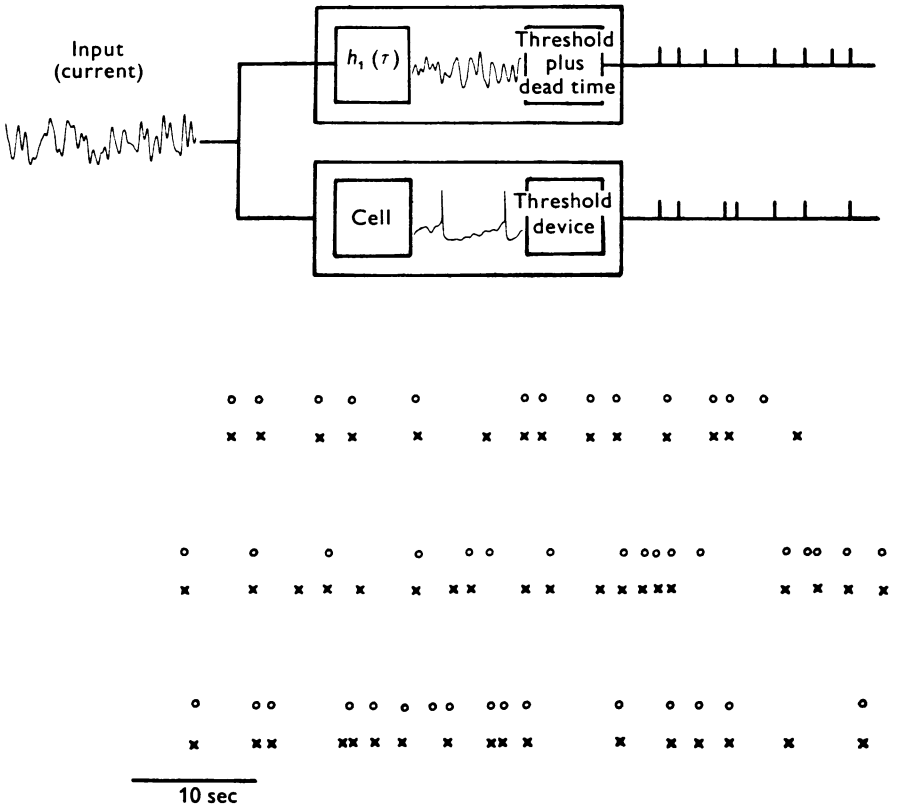

Fig. 16. Model of the current-to-spike triggering system. The first-order, linear kernel, $h_1(\tau)$ – estimated from the data – cascaded with a threshold device with a 'dead-time' was used to model the spike-triggering system. The action potential timings of the cell (×) and the model (○) to a long segment of Gaussian white-noise current show a strong correspondence.

DISCUSSION

The general question which interests us is, 'Which features of the transmembrane current are relevant in the spike-triggering process?' It is a dynamic question and relates both to inferences concerning recent stimulus history when the neurone's firing behaviour is known, and to prediction of responses when the stimulus history is known. Otherwise important investigations, by focusing on a restricted set of issues (threshold, rate of rise) and stimulating wave forms (pulses, steps, ramps), leave unanswered several aspects of the general question and have reduced value in predicting the response to other stimuli. The Wiener Gaussian white-noise method obviates these shortcomings since it effectively probes the system with

many input wave forms and results in a dynamic model with predictive capability. It has seen recent profitable use in the analysis of catfish retinal cells (Marmarelis & Naka, 1973*a*, *b*, *c*), the squid giant axon (Guttman, Feldman & Lecar, 1974), and two neuronal models (Stein, French & Holden, 1972).

Spike initiation is viewed largely as a threshold phenomenon which happens when a critical transmembrane potential or current value has been exceeded. Threshold is indeed a relevant issue, but, for a particular cell, definitely depends on the currents with which it is determined: for example, brief rectangular pulses result in higher thresholds than longer ones, slowly rising ramps may fail to excite (Lucas, 1907), and the effects of more complex stimuli are generally not known (Bennett, 1970). A significant early conclusion from the present investigation was that firing mechanisms are not precisely 'tuned' to one or even to a few stimuli. Cursory examination of individual spike-evoking trajectories (Fig. 9*B*) emphasizes that a wide range of them precede APs. (Interestingly enough, however, the cell responds with great reliability to a wide variety of wave forms, Fig. 4.) If the cell is not tuned precisely, then it is of importance to understand the significance of several statistical measures. The average current trajectory is essentially the first-order Wiener kernel and, therefore, the impulse response function of the best *linear* model of the transmembrane current-to-spike triggering system. All the trajectories exhibited common features (Figs. 6, 7, 9, 10). First, they had an expected, relatively fast and marked outward current surge close to spike initiation. Secondly, they had an earlier, slower and smaller, component which tended to oppose the overall d.c. bias. Third, they all peaked significantly earlier (40–75 msec) than the time of AP initiation. This surprising feature cannot be explained on the basis of triggering away from the soma at a current peak: conduction delay between the spike triggering zone and the soma is approximately 1 msec. Also, if the current after the peak were irrelevant to triggering, the average current trajectory should return to control values immediately (i.e. within the brief non-zero portion of the Gaussian white-noise autocorrelation). This early peak is probably due to the phase lag between voltage and current.

Guttman *et al.* (1974) have recently performed experiments on the squid giant axon using Gaussian white-noise current stimulation while monitoring membrane potential. They used 'sub-' and 'suprathereshold' stimuli and cross-correlated the membrane potential output with current input to obtain the corresponding first-order Wiener kernels (impulse response functions). They also examined the effect of d.c. bias for subthreshold stimulation and obtained impulse response functions which behaved very much as did ours (compare their Fig. 5 with our Figs. 6 and 7). Thus, it is

possible that although we used suprathreshold stimulation as input and spike train timing as output, the resulting first-order kernels may still partially reflect the current-to-transmembrane potential conversion. Finally, Guttman *et al.* (1974) compared their results to the response of the linearized Hodgkin–Huxley equations with subthreshold white-noise stimulation. They found qualitative agreement between the auto-spectrum of the axonal response to noise stimulation and the gain function of the linearized H–H equations. They did not, however, present a comparison of the corresponding phase response functions which can often be useful in deciding on the adequacy of a model. This work represents an attempt to analyse the subsystem which converts current to potential (see Fig. 1*B*), an important intermediary membrane process in the conversion of current-to-spike initiation.

An average, such as the average current trajectory, offers only partial indication of the individual trajectories from which it is calculated. APs could be evoked, for example, by only those wave forms close to the average: this would imply (for each τ) a very narrow histogram with a small $\sigma(\tau)$. Alternatively, they could be evoked by only two wave forms very different from one another and from the average: this would imply a bimodal histogram with large $\sigma(\tau)$. These hypothetical alternatives suggest the relevance of the density and the standard deviation in providing information about processes associated with spike triggering. The histograms demonstrated conclusively that the AP is not preceded by a small set of very similar current wave forms, but rather by a wide variety of them (Fig. 9*A*). Nevertheless, histograms were narrower than controls, revealing that there is indeed a 'selection' by the cell of a certain class of current trajectories.

The standard deviation $\sigma(\tau)$ of current values is of great use in helping to interpret the average current trajectory (Fig. 10). The smallest values of $\sigma(\tau)$ occur, not at the peak of the trajectory, but rather in the period ($60 < \tau < 150$ msec) corresponding to the fastest-rising portion of the late outward current phase. This indicates that the conformance of effective individual current trajectories to the average is greatest during this time. In some cases (Fig. 11*B*), the AP was preceded by an early period (580–330 msec) where, though the selected current trajectories had no average hyper- or depolarizing drift, it had oscillations which were uncommonly small. In other words, during this period the cell appeared to 'select' trajectories simply for their variability properties. The greater-than-expected values of $\sigma(\tau)$ in the period of $\tau < 60$ msec (Fig. 10) indicate that the cell 'selected' trajectories which tended to deviate exceptionally from the average. This is in sharp contrast to the earlier periods in which selected trajectories tended to conform to the average current trajectory. Because

of an argument similar to that used above, this period of hypervariability cannot be interpreted to mean that the AP was actually triggered earlier. Plotting data as in Fig. 11 emphasizes certain associations between the trajectory and $\sigma(\tau)$ which might otherwise have been missed: namely, there are periods when their relationship may be constant, rapidly varying, or absent.

The use of a correlation coefficient matrix (rather than the second-order Wiener kernel) to evaluate the role of second-order interactions in spike triggering was also very helpful in clarifying the physiological significance of the average current trajectory. Such a matrix (see Results) specifies how deviations of the current from the average trajectory at one moment are associated with deviations at later moments for those trajectories which triggered a spike. The results of the correlation analysis between inputs at two lags, like $\sigma(\tau)$, also emphasizes a central role of the average current trajectory in spike triggering. On the one hand, the negative correlations within the late outward phase (Figs. 14 and 15) indicate that, for effective trajectories, deviations from the average trajectory in one direction at one moment are 'compensated for' by deviations in the opposite sense at others. On the other hand, the positive correlations between the early inward and late outward current phases indicate that individual trajectories tend to keep on the same side of the average current trajectory. In other words, correlations suggest that the cell selects inputs whose values or whose profiles, respectively, tend to conform to the trajectory. Again, this point should not be overstressed since it is clear that a variety of trajectories can be effective (Fig. 9).

Many studies of electrogenic behaviour have stressed the accommodative properties of nerve cells, i.e. the changes in excitability as a function of subthreshold stimulation, especially as observed using current ramps (e.g. Araki & Otani, 1959; Bradley & Somjen, 1961; Sasaki & Otani, 1962; Sasaki & Oka, 1963; Ushiyama, Koizumi & Brooks, 1966; Ushiyama & Brooks, 1971; Schlue, Richter, Mauritz & Nacimiento, 1974*a*, *b*). During the period ($\tau < 150$ msec) of late outward current before a spike, very rapidly rising currents are present whose slopes are significantly larger in the depolarized than in the hyperpolarized cell (Figs. 12*B*, 13*B*). Earlier in time, smaller, nearly constant slopes are preferred which are outward for a hyperpolarized cell and inward for a depolarized cell. To our knowledge the relevance of acceleratory components of stimuli to spike triggering has not been previously investigated. This may be due partially to the difficulty of generating stimuli with a variety of well defined acceleratory components or to the problems associated with higher-order numerical differentiation (Hildebrand, 1956). The use of a Gaussian stimulus obviates the former difficulty while adequate digital smoothing

procedures assist in the latter (see Methods). Significantly high second-derivative values were encountered only within the last 210 msec before the AP (Fig. 13*C*). The role of complex and rapidly varying dynamic trajectories seems, therefore, greatest during this period.

The 'memory' of the system can be defined as the time between the emergence of a particular statistic from its confidence band and the instant when the spike is triggered. The average current trajectory typically emerges between 300 and 650 msec before triggering. The cell's 'memory' was sometimes longer when considering the standard deviation as compared to the trajectory (Fig. 11*B*). When interactions between current values at different moments before a spike (Figs. 14, 15) were measured, there were usually significant correlations as early as 1 sec before triggering.

The dependence on the d.c. bias of the estimated statistics (average current trajectory, $\sigma(\tau)$, correlation matrices, slopes, accelerations) during the period preceding spike initiation is remarkable. Recent research, using Lucas's 'minimum current gradient' as an index, has demonstrated that different nerve cells exhibit considerable variability in their accommodative power, and that individual cells also vary in this respect depending on 'circumstantial conditions', e.g. synaptic activity, level of anaesthesia, etc. (Sasaki & Otani, 1962). Of particular interest are the results of Sasaki & Oka (1963) and Schlue *et al.* (1974*b*) demonstrating that depolarization converts slowly adapting cells to rapidly adapting ones, whereas hyperpolarization has the opposite effect. Our results extend these observations by illustrating the effects of bias upon the temporal sequence of the average and other statistical requirements for spike triggering.

There appear to be three distinct phases associated with effective current trajectories. The intermediate period before the spike (approximately from 200 to 100 msec in Figs. 10, 11) has special characteristics: the average wave form becomes increasingly outward-going with large slope and acceleratory components; individual current trajectories deviate little from the average trajectory; and there are strong correlations between current pairs. It is, therefore, probable that this phase is the most critical in spike triggering. The role of the earlier period that opposes the d.c. bias may be a preparatory one of eliminating or reducing any bias effects which hinder spike initiation, as for example, cathodal or anodal depression. The period just preceding the spike ($\tau < 60$ msec) has two surprising features: the current is decreasing sharply and has greater-than-expected variability (Figs. 10*A*, 11*A*). We can offer no explanation for these and will just mentioned the possibilities that the decision to fire is not taken instantaneously but is elaborated over a certain period, and that there are associated processes with no overt electrophysiological manifestations.

A simple model consisting of a linear filter whose impulse response

function was the average current trajectory (or linear kernel) followed by a threshold device with an absolute refractory period predicts the cell's AP timing with a 68 % accuracy, suggesting that a substantial part of the non-linearities are concerned with refractoriness and threshold (Fig. 16). The addition of the second-order kernel to the model should significantly improve its predictive performance. Were the system linear, the average trajectory would represent the input signal to which, in the presence of noise, the system responded with the largest signal-to-noise ratio (Turin, 1960). To our knowledge, an analogous result has not been demonstrated for non-linear systems. Our results suggest that for non-linear systems the 'matched filter' concept might imply a whole family of preferred input trajectories whose properties are specified by the Wiener kernels or some derivate thereof (e.g. correlation matrix).

When large and small amplitude Gaussian white-noise signals were used, the maxima in the average current trajectories were 38 and 17 nA, respectively, but the average charge delivered per AP was very similar, differing only by 14 %. Thus, with only small excursions available, the cell 'selected' trajectories which, on the average, had a more prolonged early outward phase. When evaluating the spike triggering effectiveness of different wave forms, one must decide on criteria by which to describe and compare them: results of Fig. 8 suggest that the amount of delivered charge is a defensible choice.

It is desirable to summarize and to reiterate which are the justifiable conclusions that can be drawn from these experiments as to the relation between transmembrane current and spike initiation. It is licit, on the one hand, to state that stimulus amplitude, trajectory, variability, slope, acceleration, integral and second-order interactions all are relevant in spike triggering. Since the representative statistical values are not present in every individual effective trajectory, it is clear too that different stimulus features can compensate for one another and that triggering involves a complex 'pattern recognition' process. Such 'tuning' characteristics may have important functional consequences relevant to information transfer in nervous systems. The ability of d.c. bias, in turn dependent on synaptic and other influences, to modify the tuning characteristics of cells provides a simple mechanism to alter information flow through neural networks.

It is not licit, on the other hand, to infer that the wave forms that most frequently preceded the spike (e.g. those close to the average trajectory) were necessarily the most effective. Indeed, the number of times that a wave form evokes a spike depends not just on how effective it is, but also on how often it is produced by the Gaussian white noise. For example, a large rectangular pulse of outward current is well known to be highly effective, but since it is composed of values at the tail of the Gaussian

probability density, it will occur very rarely and therefore will evoke very few spikes. The question of spike-triggering effectiveness of individual wave forms is thus related to, but logically separable from, that discussed here and will be considered more extensively elsewhere (D. Brillinger, H. L. Bryant, P. Z. Marmarelis & J. P. Segundo, in preparation).

This work was supported by U.S.P.H.S. and N.S.F. grants to J.P.S. and a U.S.P.H.S. Postdoctoral Fellowship to H.L.B. We wish to express our gratitude to Drs P. Marmarelis, E. Decima and R. Lorente de Nó for their encouragement during the course of this work, and to Drs S. Hagiwara and D. Junge for helpful comments on an earlier version of the manuscript.

REFERENCES

ARAKI, T. & OTANI, T. (1959). Accommodation and local response in motoneurones of toad's spinal cord. *Jap. J. Physiol.* **9**, 69–83.

BENNETT, M. V. L. (1970). Voltage threshold in excitable cells depends on stimulus form. *J. Neurophysiol.* **33**, 585–594.

BRADLEY, K. & SOMJEN, G. G. (1961). Accommodation in motoneurones of the rat and cat. *J. Physiol.* **156**, 75–92.

BRILLINGER, D., BRYANT, H. L. & SEGUNDO, J. P. (1976). Identification of synaptic interactions. *Biol. Cybernet.* (in the Press).

BRYANT, H. L., RUIZ-MARCOS, A. & SEGUNDO, J. P. (1973). Correlations of neuronal spike discharges produced by monosynaptic connexions and by common inputs. *J. Neurophysiol.* **36**, 205–225.

BRYANT, H. L. & SEGUNDO, J. P. (1975). How does the neuronal spike trigger zone read transmembrane current? In *Testing and Identification of Non-Linear Systems*, ed. MCCANN, G. & MARMARELIS, P. Z.

DE BOER, E. (1967). Correlation studies applied to the frequency resolution of the cochlea. *J. Auditory Res.* **7**, 209–217.

DIXON, W. J. & MASSEY, F. J. (1969). *Introduction to Statistical Analysis*, 3rd edn. New York: McGraw-Hill Co.

FELLER, W. (1966). *An Introduction to Probability Theory and Its Applications*, vol. II. New York: John Wiley and Sons.

GEDULDIG, D. & JUNGE, D. (1968). Sodium and calcium components of action potentials in the *Aplysia* giant neurone. *J. Physiol.* **199**, 347–365.

GRAUBARD, K. (1973). Morphological and electrotonic properties of identified neurons of the mollusc *Aplysia californica*. Doctoral Dissertation, University of Washington, Seattle, Washington.

GUTTMAN, R., FELDMAN, L. & LECAR, H. (1974). Squid axon membrane response to white noise stimulation. *Biophys. J.* **14**, 941–955.

HILDEBRAND, F. B. (1956). *Introduction to Numerical Analysis*. New York: McGraw-Hill.

LEE, Y. W. & SCHETZEN, M. (1965). Measurement of the kernels of a non-linear system by cross-correlation. *Int. J. Control* **2**, 237–254.

LUCAS, K. (1907–1908). On the rate of variation of the exciting current as a factor in electric excitation. *J. Physiol.* **36**, 253–274.

MARMARELIS, P. Z. & NAKA, K. (1973*a*). Nonlinear analysis and synthesis of receptive-field responses in the catfish retina. I. Horizontal cell → ganglion cell chain. *J. Neurophysiol.* **36**, 605–618.

MARMARELIS, P. Z. & NAKA, K. (1973*b*). Nonlinear analysis and synthesis of receptive-field responses in the catfish retina. II. One-input white-noise analysis. *J. Neurophysiol.* **36**, 619–633.

MARMARELIS, P. Z. & NAKA, K. (1973*c*). Nonlinear analysis and synthesis of receptivefield responses in the catfish retina. III. Two-input white-noise analysis. *J. Neurophysiol.* **36**, 634–648.

MASSEY, F. J. (1951). The Kolmogorov–Smirnov test for goodness of fit. *J. Am. statist. Ass.* **46**, 68–78.

SASAKI, K. & OKA, H. (1963). Accommodation, local response and membrane potential in spinal motoneurons of the cat. *Jap. J. Physiol.* **13**, 508–522.

SASAKI, K. & OTANI, T. (1962). Accommodation in motoneurons as modified by circumstantial conditions. *Jap. J. Physiol.* **12**, 383–396.

SCHLUE, W. R., RICHTER, D. W., MAURITZ, K. H. & NACIMIENTO, A. C. (1974*a*). Responses of cat spinal motoneurone somata and axons to linearly rising currents. *J. Neurophysiol.* **37**, 303–309.

SCHLUE, W. R., RICHTER, D. W., MAURITZ, K. H. & NACIMIENTO, A. C. (1974*b*). Mechanisms of accommodation to linearly rising currents in cat spinal motoneurones. *J. Neurophysiol.* **37**, 310–315.

SEGUNDO, J. P. (1970). Communication and coding by nerve cells. In *The Neurosciences. Second Study Program*, ed. QUARTON, G., MELNECHUK, T. & SCHMIIT, F. O., pp. 561–586. New York: The Rockefeller University Press.

SEGUNDO, J. P., PERKEL, D. H. & MOORE, G. (1966). Spike probability in neurons: influence of temporal structure in the train of synaptic events. *Kybernetik* **3**, 67–82.

STEIN, R. B., FRENCH, A. S. & HOLDEN, A. V. (1972). The frequency response coherence, and information capacity of two neuronal models. *Biophys. J.* **12**, 295–322.

TAUC, L. (1962). Site of origin and propagation of spike in the giant neuron of *Aplysia*. *J. gen. Physiol.* **45**, 1077–1097.

TURIN, G. (1960). An introduction to matched filters. *I.R.E. Trans. Inf. Theory* **6**, 311–329.

USHIYAMA, J. & BROOKS, C. McC. (1971). Minimal-gradient requirements of motoneurones during post-tetanic potentiation. *Am. J. Physiol.* **220**, 1949–1955.

USHIYAMA, J., KOIZUMI, K. & BROOKS, C. McC. (1966). Accommodative reactions of neuronal elements in the spinal cord. *J. Neurophysiol.* **29**, 1028–1045.

WIENER, N. (1958). *Nonlinear Problems in Random Theory*. New York: John Wiley and Sons.